Journal of Power Sources 184 (2008) 627–632

Contents lists available at ScienceDirect

Journal of Power Sources

journal homepage: www.elsevier.com/locate/jpowsour

Short communication

# An improvement on cycling stability of Ti–V–Fe-based hydrogen storage alloys with Co substitution for Ni

He Miao, Mingxia Gao, Yongfeng Liu, Dan Zhu, Hongge Pan*

*Department of Materials Science and Engineering, Zhejiang University, Hangzhou 310027, People's Republic of China*

ARTICLE INFO

*Article history:*
Received 26 December 2007
Accepted 23 February 2008
Available online 29 February 2008

*Keywords:*
Hydrogen storage alloys
Ti–V-based alloys
Microstructures
Cycling stability
Electrochemical properties

ABSTRACT

In this work, the effects of Co substitution for Ni on the microstructures and electrochemical properties of $Ti_{0.8}Zr_{0.2}V_{2.7}Mn_{0.5}Cr_{0.6}Ni_{1.25-x}Co_xFe_{0.2}$ ($x = 0.00$–$0.25$) alloys were investigated systematically by XRD, SEM and electrochemical measurements. The structural investigations revealed that the main phases of all of the alloys were the C14 Laves phase in a three-dimensional network and the V-based solid solution phase with a dendritic structure. The lattice parameters and unit cell volumes of the two phases gradually increased with the increase of Co concentration. The relative abundance of the C14 Laves phase slightly increased from 47.3% to 49.6%, accordingly that of the V-based solid solution phase decreased, with the increase of $x$ from 0.00 to 0.25. The crystal grain of the V-based solid solution phase was obviously refined after Co substitution. The electrochemical investigations showed that the proper substitution of Co for Ni improved the cycling durability of the alloy electrodes mainly due to the suppression of both the pulverization of the alloy particles and the dissolution of the main hydrogen absorbing elements (V and Ti) into the KOH solution. The cycling stability of the alloy electrode with $x = 0.1$ was 79.8% after 200 cycles. However, the maximum discharge capacity ($C_{max}$) was decreased from 340.5 to 305.6 mAh $g^{-1}$, and the high rate dischargeability (HRD) gradually decreased from 66.8% to 55.0% with increasing $x$ from 0.00 to 0.25.



## 1. Introduction

The Ti–V-based hydrogen storage alloys, namely 'Laves phase related BCC solid solution', have been extensively investigated for the negative electrode materials due to their high discharge capacity [1–5] since they were reported by Akiba in 1995 [6,7]. However, some drawbacks, i.e., the poor electrochemical kinetics and cycling stability and the high cost, prevent them from the practical application in Ni/MH batteries. Our previous work indicated that the price of the Ti–V-based alloys should lower and the overall electrochemical properties of the alloy electrodes could be improved by the partial substitution of Fe for Cr [8]. However, the cycling stability of this type of alloys still needs to be further improved for their practical application in Ni/MH batteries.

The cycling stability is one of the important performances for the rechargeable batteries, and considerable investigations have been carried out for improving the cycling stability of the hydrogen storage alloy electrodes. It was well accepted that Co favored to the improvement of the cycling stability of the hydrogen storage electrode alloys due to the noticeable depression of the lattice expansion and pulverization of the alloy particles upon charge/discharge cycling [9–12]. Our previous work showed that the cycling stability of the La–Mg–Ni–Co type alloy electrodes was greatly improved due to the increase of the anti-pulverization ability of the alloy particles by Co substitution for Ni [10]. It is necessary to study the effects of Co on the cycling stability of the Ti–V-based alloy electrodes.

In this paper, the Ti–V-based alloy $Ti_{0.8}Zr_{0.2}V_{2.7}Mn_{0.5}Cr_{0.6}Ni_{1.25}Fe_{0.2}$, which possesses satisfactory discharge capacity and high rate dischargeability but unsatisfactory cycling stability [8] was selected as the pristine alloy. On the purpose of improving the cycling stability, Co was introduced into the alloy. The microstructures and electrochemical properties of the $Ti_{0.8}Zr_{0.2}V_{2.7}Mn_{0.5}Cr_{0.6}Ni_{1.25-x}Co_xFe_{0.2}$ ($x = 0.00$–$0.25$) alloys were investigated in detail.

## 2. Experimental

$Ti_{0.8}Zr_{0.2}V_{2.7}Mn_{0.5}Cr_{0.8}Ni_{1.25-x}Co_xFe_{0.2}$ ($x = 0.00, 0.05, 0.10, 0.15, 0.20, 0.25$) hydrogen storage alloys were prepared by induction levitation melting the constituent metals in a water-cooled copper crucible under argon atmosphere. The purity of all the constituent metals was at least 99.9%. The ingots were turned over and remelted twice for homogeneity. The as-cast alloys were mechan-

* Corresponding author. Tel.: +86 571 8795 2615; fax: +86 571 8795 2615.
*E-mail address:* hgpan@zju.edu.cn (H. Pan).

0378-7753/$ – see front matter © 2008 Elsevier B.V. All rights reserved.
doi:10.1016/j.jpowsour.2008.02.065

**Table 1**
Phase characteristics of $Ti_{0.8}Zr_{0.2}V_{2.7}Mn_{0.5}Cr_{0.6}Ni_{1.25-x}Co_xFe_{0.2}$ ($x$ = 0.00–0.25) hydrogen storage alloys

| Samples | Space group (no.) | Phase | Lattice parameters (Å) | | Unit cell volume (Å$^3$) | Phase abundance (wt%) |
|---|---|---|---|---|---|---|
| | | | $a$ | $c$ | | |
| $x$ = 0.00 | *P*63/*mmc* (194) | C14 | 4.887 | 7.950 | 164.415 | 47.3 |
| | *Im*3*m* (229) | b.c.c | 2.961 | | 25.960 | 52.7 |
| $x$ = 0.05 | *P*63/*mmc* (*194*) | C14 | 4.887 | 7.952 | 164.475 | 48.5 |
| | *Im*3*m* (229) | b.c.c | 2.962 | | 25.996 | 51.5 |
| $x$ = 0.10 | *P*63/*mmc* (194) | C14 | 4.887 | 7.953 | 164.493 | 48.7 |
| | *Im*3*m* (229) | b.c.c | 2.963 | | 26.004 | 51.3 |
| $x$ = 0.15 | *P*63/*mmc* (194) | C14 | 4.888 | 7.954 | 164.562 | 48.8 |
| | *Im*3*m* (229) | b.c.c | 2.964 | | 26.040 | 51.2 |
| $x$ = 0.20 | *P*63/*mmc* (194) | C14 | 4.888 | 7.955 | 164.603 | 49.0 |
| | *Im*3*m* (229) | b.c.c | 2.965 | | 26.066 | 51.0 |
| $x$ = 0.25 | *P*63/*mmc* (194) | C14 | 4.889 | 7.956 | 164.660 | 49.6 |
| | *Im*3*m* (229) | b.c.c | 2.966 | | 26.079 | 50.4 |

ically crushed and ground into powder of 300 mesh size (≤50 μm) for X-ray diffraction (XRD) and the electrochemical measurements.

The microstructures and the electrochemical properties except for the cycling stability were investigated by the same methods as described in our previous paper [8]. The cycle life of the alloy electrodes was tested by charging the electrode at 300 mA g$^{-1}$ for 2 h followed by a 10 min break, and then discharging the electrode at 300 mA g$^{-1}$ to the cut-off potential of −0.6 V vs. the Hg/HgO reference electrode. To investigate the dissolution of Ti and V elements in the alkaline electrolyte, the KOH solution was analyzed after 100 and 200 cycles by a 721-type spectrophotometer. The morphology of the alloy particles after 200 cycles was observed by the FEI-SLRION scanning electron microscope (SEM).

## 3. Results and discussion

### 3.1. Microstructures

Fig. 1 shows the XRD patterns of $Ti_{0.8}Zr_{0.2}V_{2.7}Mn_{0.5}Cr_{0.8}Ni_{1.25-x}Co_xFe_{0.2}$ ($x$ = 0.00–0.25) alloys. Apparently, all of the alloys mainly consist of a C14 Laves phase with $MgZn_2$-type hexagonal structure and a V-based solid solution phase with BCC structure. Table 1 lists the relative abundance, the lattice parameters and the unit cell volumes of the two phases calculated by Rietveld analysis. With the increase of Co content, the lattice parameters and the unit cell volumes of these two phases are slightly increased due to the larger atom radius of Co (1.67 Å) than that of Ni (1.62 Å). The relative abundance of the C14 Laves phase in the alloys slightly increases from 47.3% to 49.6% with increasing $x$ from 0.00 to 0.25, accordingly that of the V-based solid solution phase decreases from 52.7% to 50.4%.

Fig. 2(a)–(d) shows SEM (BSE model) images of the $Ti_{0.8}Zr_{0.2}V_{2.7}Mn_{0.5}Cr_{0.8}Ni_{1.25-x}Co_xFe_{0.2}$ ($x$ = 0.00, 0.05, 0.15, 0.25) alloys. EDS analyses indicate that the dark grey dendritic crystal

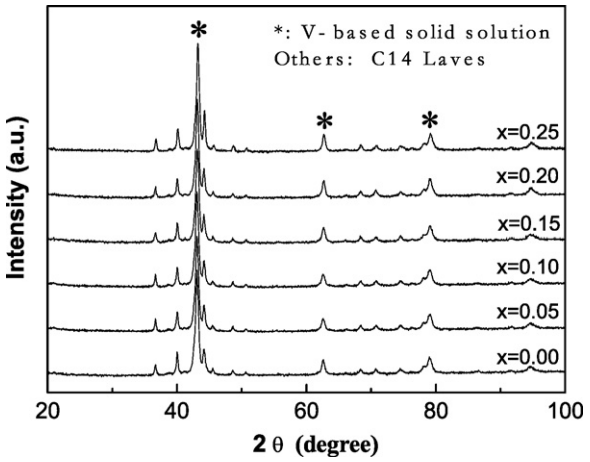


**Fig. 1.** XRD patterns of $Ti_{0.8}Zr_{0.2}V_{2.7}Mn_{0.5}Cr_{0.6}Ni_{1.25-x}Co_xFe_{0.2}$ ($x$ = 0.00–0.25) alloys.

is the V-based solid solution phase and the light grey 3D network structural phase is the C14 Laves phase as reported in our previous work [8]. By comparison, it can be found that the crystal grain size of the V-based solid solution phase gradually decreases with increasing Co content as shown in Fig. 2, indicating the substitution of Co for Ni can effectively refine the crystal grain of V-based solid solution phase in the Ti–V-based alloys.

### 3.2. Discharge capacity and cycling stability

Values of the maximum discharge capacity of $Ti_{0.8}Zr_{0.2}V_{2.7}Mn_{0.5}Cr_{0.8}Ni_{1.25-x}Co_xFe_{0.2}$ ($x$ = 0.00–0.25) alloy electrodes are presented in Table 2. With increasing $x$ from 0.00 to 0.25, the maximum discharge capacity ($C_{max}$) decreases gradually from

**Table 2**
Electrochemical characteristics of $Ti_{0.8}Zr_{0.2}V_{2.7}Mn_{0.5}Cr_{0.6}Ni_{1.25-x}Co_xFe_{0.2}$ ($x$ = 0.00–0.25) hydrogen storage alloys at 303 K

| Samples | $C_{max}$ (mAh g$^{-1}$) | Cycling stability ($S_{200}$) (%) | $HRD_{600}$ (%) | $I_0$ (mA g$^{-1}$) | | $\Delta I_0/I_0^{25}$ (%) |
|---|---|---|---|---|---|---|
| | | | | 25 cycles | 200 cycles | |
| $x$ = 0.00 | 340.5 | 73.5 | 66.8 | 139.4 | 70.9 | 49.1 |
| $x$ = 0.05 | 337.9 | 76.2 | 64.9 | | | |
| $x$ = 0.10 | 333.4 | 79.8 | 62.5 | 120.7 | 78.3 | 35.0 |
| $x$ = 0.15 | 322.2 | 79.3 | 59.9 | | | |
| $x$ = 0.20 | 314.6 | 77.6 | 57.8 | 104.9 | 94.3 | 10.2 |
| $x$ = 0.25 | 305.6 | 74.4 | 55.0 | | | |

*Note*: $HRD_{600}$: the high rate dischargeability with discharge current density $I_d$ = 600 mA g$^{-1}$. $\Delta I_0/I_0^{25}$ : $\Delta I_0/I_0^{25} = (I_0^{25} - I_0^{200})/I_0^{25}$ ($I_0^{25}$ and $I_0^{200}$ are the $I_0$ of the alloy electrodes after 25 and 200 charge/discharge cycles, respectively).

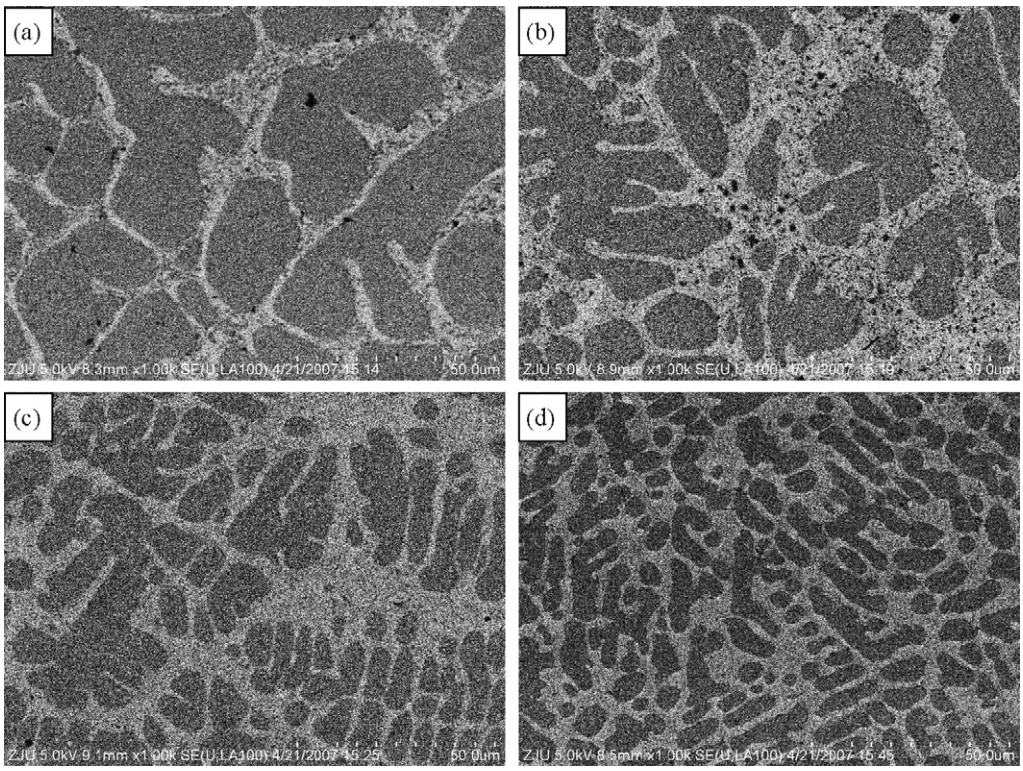


**Fig. 2.** SEM images of $Ti_{0.8}Zr_{0.2}V_{2.7}Mn_{0.5}Cr_{0.6}Ni_{1.25-x}Co_xFe_{0.2}$ ($x = 0.00, 0.05, 0.15, 0.25$) alloys.

340.5 to 305.6 mAh $g^{-1}$, indicating a monotonic decrease of the $C_{max}$ of the alloy electrodes with increasing the content of the substitution of Co for Ni. It is well known that Ni is an indispensable element in hydrogen storage electrode alloys due to their high electrocatalytic activity [13]. In present study, the decrease of the maximum discharge capacity should be related to the decrease of electrocatalytic activity of the alloy electrode with Co substitution for Ni.

Fig. 3 shows the discharge capacity vs. cycle number of the $Ti_{0.8}Zr_{0.2}V_{2.7}Mn_{0.5}Cr_{0.8}Ni_{1.25-x}Co_xFe_{0.2}$ ($x = 0.00$–$0.25$) alloy electrodes. In present study, the cycling stability of the alloy electrodes is evaluated by the retention of the discharge capacity after 200 charge/discharge cycles ($C_{200}/C_{max}$). The values of $C_{200}/C_{max}$ of the alloy electrodes are also listed in Table 2. Apparently, the $C_{200}/C_{max}$ of the alloy electrodes increases from 73.5% ($x = 0.0$) to 79.8% ($x = 0.10$) and then drops to 74.4% ($x = 0.25$) with increasing Co content. This result indicates that the proper substitution of Co for Ni can effectively improve the cycling stability of the alloy electrodes. The pulverization of the alloy particles and corrosion/oxidation of the active compositions of the alloys are two main factors responsible for the degradation of the discharge capacity of the hydrogen storage alloy electrodes. In order to ascertain the improvement mechanism of the cycling stability of the alloy electrodes with Co substitution for Ni, the investigations on the pulverization of the alloy particles and the corrosion of the active compositions of the alloys were carried out.

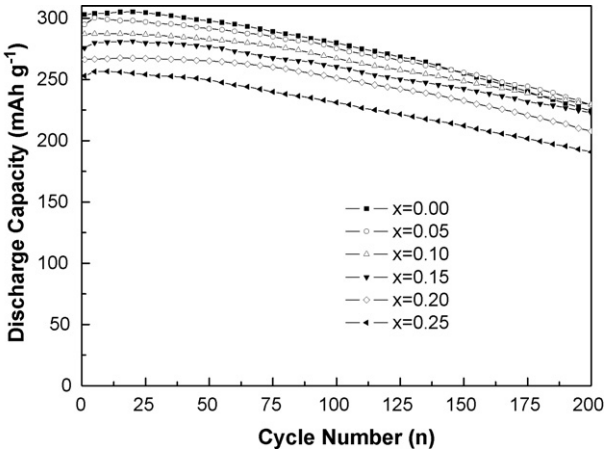


**Fig. 3.** Cycling stability of $Ti_{0.8}Zr_{0.2}V_{2.7}Mn_{0.5}Cr_{0.6}Ni_{1.25-x}Co_xFe_{0.2}$ ($x = 0.00$–$0.25$) alloy electrodes at 303 K.

Fig. 4 shows the SEM micrographs of the $Ti_{0.8}Zr_{0.2}V_{2.7}Mn_{0.5}Cr_{0.8}Ni_{1.25-x}Co_xFe_{0.2}$ ($x = 0.00$, 0.10, 0.20) alloys after 200 charge/discharge cycles. It is obvious that the microcracks were generated after 200 cycles due to the pulverization of the alloy particles caused by the volume expansion and shrinkage during hydrogenation and dehydrogenation. The generation of the microcracks in the alloy particles or the pulverization of the alloy particles increases the contact resistance and decreases the conductivity between alloy particles, which subsequently degrades the discharge capacity of the alloy electrodes. With increasing Co content, the pulverization of the alloy particles is weakened, revealing that the substitution of Co for Ni can effectively suppress the pulverization of the alloy particles. Co is well known as an element suppressing pulverization of the alloy particles by decreasing the cell volume expansion of the hydrogen absorbing phases in the hydrogen storage alloys [14]. Moreover, the crystal grain refinement can also increase the pulverization resistance of the hydrogen storage alloys as reported by Li and Wang [15]. All these may be responsible for the suppression of the pulverization of the alloy particles with higher Co content during charge/discharge.

Fig. 5 shows the dissolution of the Ti and V elements from $Ti_{0.8}Zr_{0.2}V_{2.7}Mn_{0.5}Cr_{0.8}Ni_{1.25-x}Co_xFe_{0.2}$ ($x = 0.00$, 0.10, 0.20) alloy electrodes into the electrolyte after 100 and 200 charge/discharge cycles. Ti and V were detected in the KOH solution after cycling, and they were corroded and dissolved into the KOH solution. With

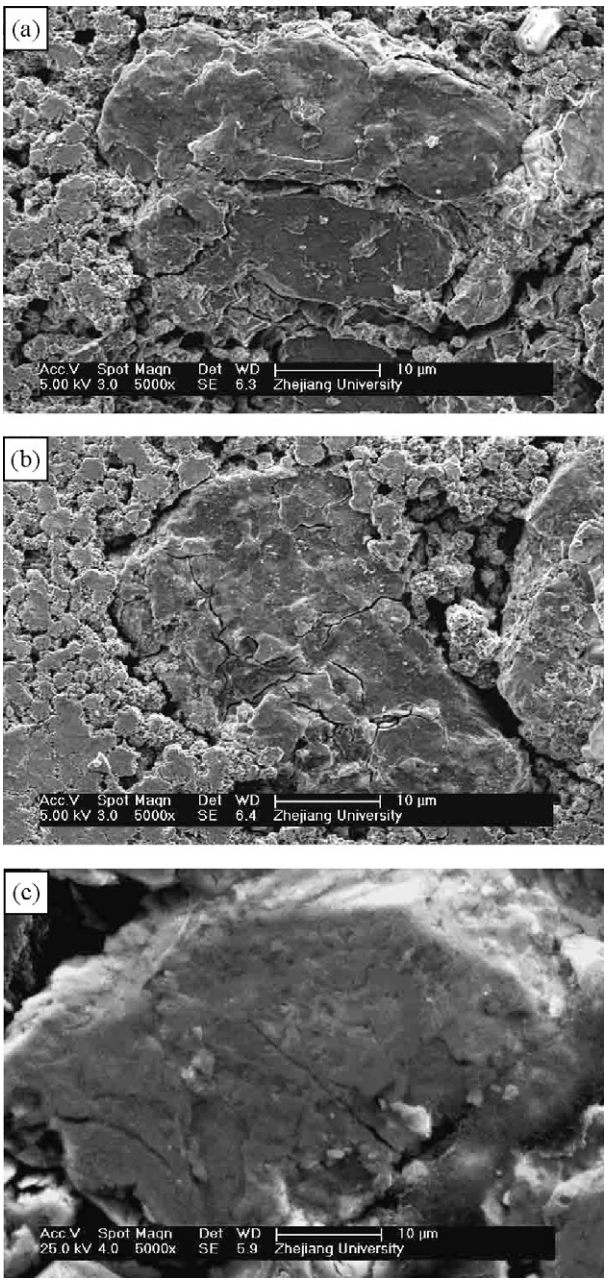


**Fig. 4.** SEM images of $Ti_{0.8}Zr_{0.2}V_{2.7}Mn_{0.5}Cr_{0.6}Ni_{1.25-x}Co_xFe_{0.2}$ ($x$ = 0.00, 0.10, 0.20) alloy particles after 200 cycles.

increasing cycle number from 100 to 200, the dissolution of Ti and V was increased as shown in Fig. 5. Furthermore, it can be seen from Fig. 5, with an addition of Co of $x$ = 0.1, the amount of Ti and V dissolved in the KOH solution decreased but further increase of the Co content to $x$ = 0.2, the dissolution increased. The phenomenon suggests that the proper substitution of Co for Ni can inhibit the dissolution of the Ti and V in the alkaline solution, which can be ascribed to the suppression of the pulverization during the charge/discharge cycling. But the excessive decrease of Ni content caused by the excessive Co substitution would accelerate the dissolution of the V-based solid solution phase in the alkaline solution due to the loss of the electrocatalytic activity [2,16].

The linear polarization curves of the $Ti_{0.8}Zr_{0.2}V_{2.7}Mn_{0.5}Cr_{0.8}Ni_{1.25-x}Co_xFe_{0.2}$ ($x$ = 0.00, 0.10, 0.20) alloy electrodes are shown in Fig. 6. A linear dependence between the polarization current and the overpotential exists when the overpotential is changed within

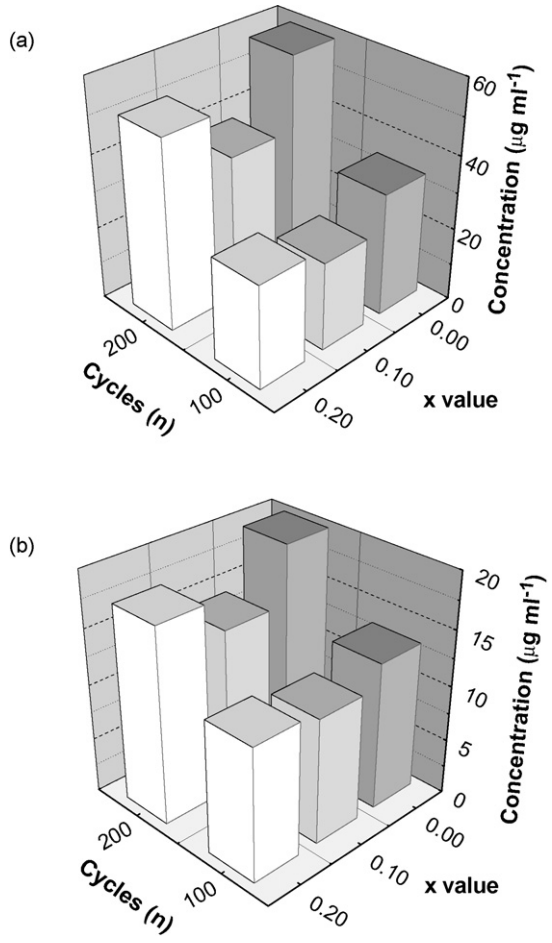


**Fig. 5.** Dissolution amount of V (a) and Ti (b) elements of $Ti_{0.8}Zr_{0.2}V_{2.7}Mn_{0.5}Cr_{0.6}Ni_{1.25-x}Co_xFe_{0.2}$ ($x$ = 0.00, 0.10, 0.20) alloys after 100 and 200 cycles.

a small range. The values of the exchange current density $I_0$ calculating by the following equation [17]:

$$I_0 = \frac{IRT}{F\eta} \quad (2)$$

are also presented in Table 2, where $I$, $R$, $T$, $F$, $\eta$ denote the polarization current density, the gas constant, the absolute temperature, the Faraday constant and the overpotential, respectively. The exchange

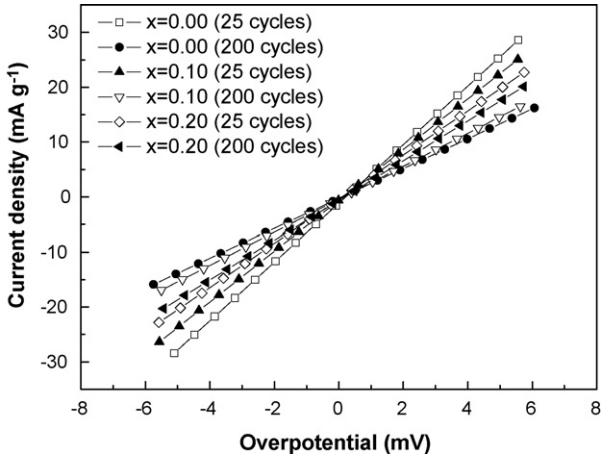


**Fig. 6.** Linear polarization curves of $Ti_{0.8}Zr_{0.2}V_{2.7}Mn_{0.5}Cr_{0.6}Ni_{1.25-x}Co_xFe_{0.2}$ ($x$ = 0.00, 0.10, 0.20) alloy electrodes after 25 and 200 cycles at 303 K.

current density ($I_0$) of the hydrogen storage alloy electrodes represents the charge-transfer reaction rate of hydrogen on the surface of the alloy electrodes. As can be seen in Table 2, the $I_0$ of the alloy electrodes decreases obviously with increasing the charge/discharge cycles from 25 to 200, implying that the charge-transfer reaction rate was decreased with cycling. In order to evaluate the effect of Co on the charge-transfer reaction rate of the alloy electrodes, the decreasing extent of the charge-transfer reaction rate ($\Delta I_0/I_0^{25}$) was calculated and listed in Table 2. It is obvious that $\Delta I_0/I_0^{25}$ decreases from 49.1% to 10.2% with increasing $x$ from 0.00 to 0.20. This result indicates that the substitution of Co for Ni can effectively suppress the decrease of the charge-transfer reaction rate on the surface of the alloy electrodes during cycling.

### 3.3. HRD and EIS

Fig. 7 shows the high rate dischargeability (HRD) of the $Ti_{0.8}Zr_{0.2}V_{2.7}Mn_{0.5}Cr_{0.8}Ni_{1.25-x}Co_xFe_{0.2}$ ($x$ = 0.00–0.25) alloy electrodes. The HRD is defined and calculated according to the following equation:

$$\mathrm{HRD}\,(\%) = \frac{C_\mathrm{d}}{C_\mathrm{d} + C_{60}} \times 100 \quad (1)$$

where $C_\mathrm{d}$ is the discharge capacity with a cut-off potential of −0.6 V vs. Hg/HgO reference electrode at the discharge current density $I_\mathrm{d}$, $C_{60}$ is the residual discharge capacity with the cut-off potential of −0.6 V vs. Hg/HgO reference electrode at the discharge current density $I_{60}$ after the alloy electrode has been fully discharged at $I_\mathrm{d}$. As can be seen from Fig. 7, the HRD of the alloy electrodes decreases gradually with increasing $x$. The $HRD_{600}$ value of the alloy electrodes listed in Table 2 decreases from 66.8% to 55.0%. In general, the HRD represents the electrochemical kinetics of the alloy electrodes which is related to the charge-transfer rate occurring at the electrode surface and the diffusion rate of hydrogen atom. The charge-transfer reaction rate can be evaluated by the charge-transfer reaction resistance ($R_\mathrm{ct}$) on the alloy electrode surface, which can be measured by electrochemical impedance spectra (EIS).

Fig. 8 shows EIS of the $Ti_{0.8}Zr_{0.2}V_{2.7}Mn_{0.5}Cr_{0.8}Ni_{1.25-x}Co_xFe_{0.2}$ ($x$ = 0.00–0.25) alloy electrodes. The smaller semicircle (semicircle 1) in the high-frequency region relates the contact resistance between the alloy powder and the conductive material, and the larger semicircle (semicircle 2) in the low-frequency region relates the charge-transfer resistance ($R_\mathrm{ct}$) on the alloy electrode surface [18]. With increasing Co content, the radius of semicircle 1 keeps almost unchanged, indicating that the contact resistance between the alloy powder and the conductive material keeps unchanged. Whereas, the radius of semicircle 2 increases gradually with the increase of $x$, implying that the $R_\mathrm{ct}$ increases after the substitution of Co for Ni. The substitution of Co for Ni decreases the Ni content in the alloys, which may induce the drop of the electrocatalytic activity of the alloy electrode [13]. This may be one of the reasons for the deterioration of the HRD of the alloy electrodes after the substitution of Co for Ni.

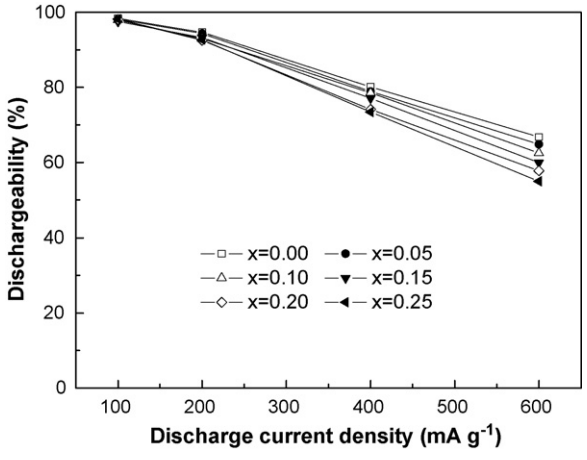


**Fig. 7.** High rate dischargeability of $Ti_{0.8}Zr_{0.2}V_{2.7}Mn_{0.5}Cr_{0.6}Ni_{1.25-x}Co_xFe_{0.2}$ ($x$ = 0.00–0.25) alloy electrodes at 303 K.

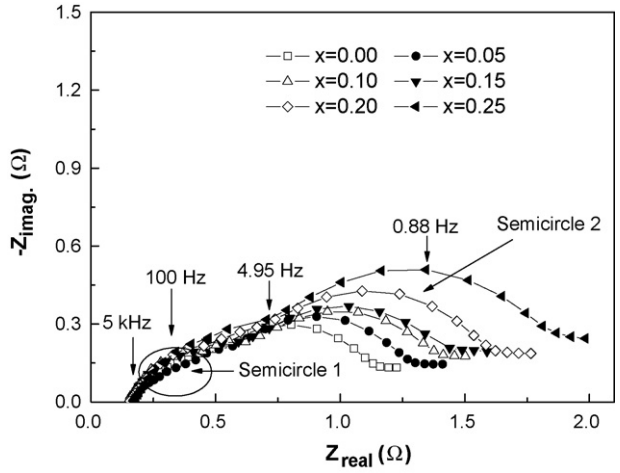


**Fig. 8.** Electrochemical impedance spectra (EIS) of the $Ti_{0.8}Zr_{0.2}V_{2.7}Mn_{0.5}Cr_{0.6}Ni_{1.25-x}Co_xFe_{0.2}$ ($x$ = 0.00–0.25) alloy electrodes at 303 K.

## 4. Conclusions

The effects of the substitution of Co for Ni on the microstructures and electrochemical properties, especially the cycling stability of the $Ti_{0.8}Zr_{0.2}V_{2.7}Mn_{0.5}Cr_{0.8}Ni_{1.25-x}Co_xFe_{0.2}$ ($x$ = 0.00–0.25) alloys were investigated systematically, the main conclusions can be drawn as the following:

1. The alloys consist mainly a C14 Laves phase with three-dimensional network structure and a V-based solid solution phase with dendritic structure. With increasing Co content, the lattice parameters and unit cell volumes of these two phases increase, and the grain size of the V-based phase decreases. The relative abundance of the C14 Laves phase increases slightly, accordingly that of the V-based solid solution phase decreases with the increase of Co content.
2. The cycling stability ($C_{200}/C_\mathrm{max}$) of the alloy electrodes increases firstly from 73.5% ($x$ = 0.00) to 79.8% ($x$ = 0.10), and then slightly decreases to 74.4% ($x$ = 0.25). The improvement of the cycling stability can be attributed to the suppression of both the pulverization of the alloy particles and dissolution of the Ti and V elements of the alloy electrodes by the suitable amount of the substitution of Co for Ni. Excessive substitution of Co for Ni increases the dissolution of Ti and V elements thus decreases the cycling stability of the alloy.
3. The maximum discharge capacity of the alloy electrodes decreases from 340.5 ($x$ = 0.00) to 305.6 mAh $g^{-1}$ ($x$ = 0.25). The HRD of the alloy electrodes shows a decreasing tendency with the increase of Co content due to the increase of the charge-transfer resistance on the surface of the alloy electrodes caused by the loss of the electrocatalytic activity.

## Acknowledgements

This work was financially supported by the National Natural Foundation of China (50471040) and Program for New Century Excellent Talents in University (NCET-06-0519).

## References

[1] H. Iba, E. Akiba, J. Alloys Compd. 253–254 (1997) 21–24.
[2] M. Tsukahara, K. Takahashi, T. Mishima, T. Sakai, H. Miyamura, N. Kuriyama, I. Uehara, J. Alloys Compd. 226 (1995) 203–207.
[3] M. Tsukahara, K. Takahashia, T. Mishima, A. Isomura, T. Sakai, J. Alloys Compd. 253–254 (1997) 583–586.
[4] H.G. Pan, R. Li, M.X. Gao, Y.F. Liu, Y.F. Lei, Q.D. Wang, Int. J. Hydrogen Energy 31 (2006) 1188–1195.
[5] Y.F. Zhu, H.G. Pan, M.X. Gao, J.X. Ma, Y.Q. Lei, Q.D. Wang, Int. J. Hydrogen Energy 28 (2003) 311–316.
[6] H. Iba, E. Akiba, J. Alloys Compd. 231 (1995) 508–512.
[7] M. Yoshida, E. Akiba, J. Alloys Compd. 224 (1995) 121–126.
[8] H. Miao, M.X. Gao, Y.F. Liu, Y. Lin, J.H. Wang, H.G. Pan, Int. J. Hydrogen Energy 32 (2007) 3947–3953.
[9] L.X. Chen, R. Guo, Y.Q. Lei, L. Li, Q.D. Wang, Mater. Chem. Phys. 92 (2005) 554–558.
[10] Y.F. Liu, H.G. Pan, M.X. Gao, R. Li, Y.Q. Lei, J. Alloys Compd. 376 (2004) 304–313.
[11] Y.F. Liu, H.G. Pan, Y.J. Yue, X.F. Wu, N. Chen, Y.Q. Lei, J. Alloys Compd. 395 (2005) 291–299.
[12] J.M. Cocciantelli, P. Bernard, S. Fernandez, J. Atkin, J. Alloys Compd. 253–254 (1997) 642–647.
[13] J. Kleperis, G. Wojcik, A. Czerwinski, J. Skowronski, M. Kopezyk, M. Beltowska-Brzezinska, J. Solid State Electrochem. 5 (2001) 229.
[14] J.J.G. Willems, Philips J. Res. 39 (1984) 1–94.
[15] C.J. Li, X.L. Wang, J. Alloys Compd. 270 (1998) 246–254.
[16] D.Y. Yan, G. Sandrock, S. Suda, J. Alloys Compd. 223 (1995) 32–38.
[17] P.H.L. Notten, P. Hokkeling, J. Elecrochem. Soc. 138 (1991) 1877–1885.
[18] N. Kuriyama, T. Sakai, H. Miyamura, I. Uehara, H. Ishikawa, T. Iwasaki, J. Alloys Compd. 202 (1993) 183–197.